1226 *Biochemistry* **2011,** *50,* 1226–1237
DOI: 10.1021/bi101432p

BIOCHEMISTRY
including biophysical chemistry & molecular biology
Article

Improving a Designed Photocontrolled DNA-Binding Protein†

Helen Y. Fan,‡ Stacy-Anne Morgan,§ Katherine E. Brechun,§ Yih-Yang Chen,‡ Anna S. I. Jaikaran,§ and G. Andrew Woolley*,§

‡*Faculty of Engineering, University of Waterloo, 200 University Avenue West, Waterloo, Ontario, Canada N2L 3G1, and* §*Department of Chemistry, University of Toronto, 80 St. George Street, Toronto, Ontario M5S 3H6, Canada*

Received September 4, 2010; Revised Manuscript Received January 6, 2011

ABSTRACT: Photocontrolled transcription factors could be powerful tools for probing the roles of transcriptional processes in a variety of settings. Previously, we designed a photocontrolled DNA-binding protein based on a fusion between the bZIP region of GCN4 and photoactive yellow protein from *Halorhodospira halophila* [Morgan, S. A., et al. (2010) *J. Mol. Biol. 399*, 94−112]. Here we report a structure-based attempt to improve the degree of photoswitching observed with this chimeric protein. Using computational design tools PoPMuSiC 2.0, Rosetta, Eris, and bCIPA, we identified a series of single- and multiple-point mutations that were expected to stabilize the folded dark state of the protein and thereby enhance the degree of photoswitching. While a number of these mutations, particularly those that introduced a hydrophobic residue at position 143, did significantly enhance dark-state protein stability as judged by urea denaturation studies, dark-state stability did not correlate directly with the degree of photoswitching. Instead, the influence of mutations on the degree of photoswitching was found to be related to their effects on the degree to which DNA binding slowed the pB to pG transition in the PYP photocycle. One mutant, K143F, caused an ∼10-fold slowing of the photocycle and also showed the largest difference in the apparent K_d for DNA binding, 3.5-fold lower, upon irradiation. This change in the apparent K_d causes a 12-fold enhancement in the fraction bound DNA upon irradiation due to the cooperativity of DNA binding by this family of proteins. The results highlight the strengths and weaknesses of current approaches to a practical problem in protein design and suggest strategies for further improvement of designed photocontrolled transcription factors.

Photocontrol of transcriptional processes in living cells may help to elucidate the roles of location and timing of gene expression in spatiotemporally complex settings that occur during development and during normal functioning of the nervous system (*1*). Naturally occurring photocontrolled transcription factors are known (*2*, *3*); however, they are often multicomponent systems, so that engineering them for use as tools for the photocontrol of transcription is not straightforward. Alternatively, naturally occurring light-dependent protein−protein interactions may be co-opted to photocontrol transcription. Quail and colleagues used a phytochrome−GAL4−DNA-binding domain fusion and a PIF3−GAL4−activation domain fusion to photocontrol the expression of genes that contain a promoter with a GAL4 binding site (*4*). A similar approach using the transactivator VP16 fused to the LOV domain of FKF1 and the partner protein GIGANTEA fused to the GAL4 DNA binding domain was reported by Yazawa et al. (*5*). In an elegant, structure-based approach to the creation of a light-activated DNA-binding protein, Strickland et al. linked a LOV domain to the Trp repressor via a shared α-helix (*6*, *7*). In their design, the helix is expected to be packed against the LOV domain in the dark and thus cannot adopt its normal location in the Trp repressor, inhibiting Trp repressor DNA binding ability. Upon irradiation, the helix detaches from the LOV domain to rejoin the Trp repressor, thereby activating it.

We recently reported a conceptually similar design of a photocontrolled bZIP-type DNA-binding protein (GCN4Δ25PYP-v2) that is a hybrid of the prototypical homodimeric bZIP DNA-binding protein GCN4 and photoactive yellow protein (PYP),[1] a blue light sensitive protein from *Halorhodospira halophila* (*8*). A fusion of the C-terminal coiled-coil region of GCN4 bZIP with the N-terminal cap of PYP was made on the basis of examination of available crystal structure data, analysis of amino acid preference rules for coiled coils, mutational and amino acid conservation data for PYP, and with Rosetta-guided structural modeling. GCN4Δ25PYP-v2 is monomeric in the dark, and fluorescence and circular dichroism data indicate the coiled-coil domain is hidden. Binding to target DNA in the dark causes substantial structural reorganization of GCN4Δ25PYP-v2 with a concomitant slowing of the photocycle consistent with conformational coupling of the DNA-binding and light-sensitive domains of the protein. Blue light irradiation caused a 2-fold decrease in the apparent K_d for specific DNA binding that was reversed in the dark. Although this effect was reproducible and reversible, a more substantial difference in DNA binding between dark and light states would be preferable if such designs are to

†We thank the Natural Sciences and Engineering Research Council of Canada, the Canadian Institutes of Health Research, and the National Institutes of Health (R01 MH086379) for financial support.

*To whom correspondence should be addressed: Department of Chemistry, University of Toronto, 80 St. George St., Toronto, Ontario M5S 3H6, Canada. E-mail: awoolley@chem.utoronto.ca. Telephone: (416) 978-0675. Fax: (416) 978-8775.

[1]Abbreviations: PYP, photoactive yellow protein; bZIP, basic leucine zipper; PCR, polymerase chain reaction; SDS−PAGE, sodium dodecyl sulfate−polyacrylamide gel electrophoresis; ESI-MS, electrospray ionization mass spectrometry; EDTA, ethylenediaminetetraacetic acid.

 Published on Web 01/10/2011

be useful as tools for controlling DNA binding and transcription in vivo.

If a suitable selection or screening approach were devised, random mutagenesis might be expected to yield GCN4Δ25PYP variants with improved photoswitching behavior. A consequence of the structure-based approach, however, is that the structure may help narrow the search for proteins with improved properties. Here we focus on efforts to stabilize the hybrid N-terminal cap of GCN4Δ25PYP-v2 in its dark state by seeking to optimize packing interactions between the hybrid cap and its docking sites on the PYP core with the anticipation that this may lead to larger differences in DNA binding upon irradiation. Stabilization of a well-defined folded structure by targeted mutation is a task considered amenable to computational modeling techniques (*9*, *10*). Here we have used several such computational approaches to design a small set of GCN4Δ25PYP variants. These proteins were expressed and their dark-state stabilities as well as their photoswitching behaviors were characterized in detail.

MATERIALS AND METHODS

Site-Directed Mutagenesis. Primers for the mutations were designed with PrimerX (http://www.bioinformatics.org/primerx/) following the Stratagene QuikChange protocol (Agilent, Inc.) and purchased from ACGT Corp. For each mutation, 125 ng each of the forward and reverse primers were added to 100 ng of template DNA, 1 μL of dNTPs, 5 μL of DMSO, 1 μL of Pfu polymerase (Fermentas), 5 μL of 10× Pfu reaction buffer with $MgSO_4$, and water in a total volume of 50 μL. A drop of mineral oil was also added to prevent evaporation. The reaction mixture was held at (i) 95 °C for 30 s followed by (ii) 30 s at 95 °C, (iii) 1 min at 5 °C below the primer T_m, and (iv) 7.5 min at 72 °C. Steps ii−iv were repeated 18 times. Then the mixture was held at (v) 72 °C for an additional 20 min before being allowed to cool to room temperature. A 1 μL aliquot of DpnI was added to the reaction mixture, which was then incubated at 37 °C for 1 h. A 0.8% agarose gel in 0.5× TBE was then run to check for PCR products. A PCR purification kit (Invitrogen) was subsequently used, and the product was transformed into XL-2 Blue Ultracompetent cells. A midiprep (Invitrogen) was conducted, and the plasmids were sequenced in both directions (ACGT Corp.) to confirm the mutations.

Protein Expression and Purification. The expression and reconstitution of the PYP constructs were adapted from the work of Devanathan et al. (*11*). The protocol was the same for all constructs. DNA (0.2 ng) was transformed into BL21*(DE3) competent cells and plated onto agar plates containing 30 μg/mL kanamycin. The following day, a single colony was used to inoculate 25 mL of Luria-Bertani (LB) broth that had been supplemented with kanamycin (30 μg/mL) and grown overnight at 37 °C. The 25 mL overnight culture was subsequently used to inoculate 1 L of LB supplemented with 30 μg/mL kanamycin. Cells were grown at 37 °C until an OD of 0.6 had been reached and then induced with 1 mM IPTG. The temperature was adjusted to 25 °C, and the cells were grown for a further 1.5 h before 30 mg of activated chromophore dissolved in 1 mL of ethanol was added to the medium. The synthesis of the activated chromophore, 4-hydroxycinnamic acid thiophenyl ester, was conducted as detailed by Changenet-Barret et al. (*12*) except that the product used for the reconstitution of holoprotein was not recrystallized. The cells were grown for a further 6 h before centrifugation to separate the medium from the protein-containing cell pellet.

The pellet was resuspended in buffer containing 50 mM sodium phosphate (pH 8.0), 300 mM sodium chloride, and 5 mM magnesium chloride and frozen at −20 °C until purification was conducted. The resuspended cell pellet was sonicated in pulses on ice for 5 min and then centrifuged at 18K for 30 min to separate the supernatant from the pellet. The protein was purified on a Ni-NTA column that was equilibrated with lysis buffer. After addition of the protein-containing supernatant, the resin was washed with 10 column volumes (CV) of the lysis buffer. The resin was subsequently washed with 5 CV of high-salt buffer (i.e., lysis buffer supplemented with 2 M NaCl) followed by a further 5 CV of lysis buffer. To elute nonspecifically bound proteins, the resin was subjected to 5 CV of lysis buffer supplemented with 5 mM imidazole. The protein was eluted by increasing the imidazole concentration to 200 mM.

The eluted protein was dialyzed extensively against 40 mM Tris-OAc, 1 mM EDTA, and 100 mM NaCl (pH 7.5) [1× TAE, 100 mM NaCl (pH 7.5)]. The dialyzed protein was concentrated to ∼1.5 mL using an Amicon ultracentrifugal device (10000 Da NMWL) (Millipore). The purity of the samples was confirmed using 12.5% SDS−PAGE and ESI-MS. Where further purification was required, the protein was applied to a Superdex 75 column running in 1× TAE, 100 mM NaCl (pH 7.5) at 4 °C. UV−vis absorbance spectroscopy was used to determine which eluted fractions had the highest ratios of absorbance at 446 nm to that at 278 nm.

Target DNA. The following oligomers were used for annealing AP-1 duplexes: AP1_S1, 5′ TCC GGA TGA CTC ATT TTT TG 3′; Cy3_AP1_S1, 5′ Cy3-TCC GGA TGA CTC ATT TTT TG 3′; AP1_S2, 5′ CAA AAA ATG AGT CAT CCG GA 3′. A 1:1 ratio of each unlabeled oligonucleotide in 10 mM Tris-HCl, 50 mM NaCl, and 1 mM EDTA (pH 7.6) was heated in a water bath to 80 °C for 10 min. After 10 min, the hot plate was turned off and the DNA allowed to slowly cool to room temperature. For labeled AP-1 DNA, a 1:1.2 ratio of labeled to unlabeled oligonucleotide was used.

UV−Vis Spectra and Photoisomerization. UV−vis spectra of the proteins were recorded in 1× TAE, 100 mM NaCl (pH 7.5) at 20 °C in a 1.0 cm path length quartz cuvette using a PE Lambda 35 spectrophotometer. Protein concentrations were determined using an extinction coefficient at λ_{max} (∼446 nm) of 45 mM^{-1} cm^{-1}. Samples for thermal relaxation were prepared at a final protein concentration of 5 μM in 1× TAE, 100 mM NaCl (pH 7.5). The protein samples with nonspecific DNA consisted of the same 5 μM protein in 1× TAE, 100 mM NaCl (pH 7.5) but with sheared salmon testes DNA added to a final concentration of 1 mg/mL. Samples with target DNA contained in addition to the salmon testes DNA, an equimolar (i.e., 5 μM) amount of annealed AP-1 DNA duplex. Irradiation of the protein sample was conducted by using a Luxeon III Star LED Royal Blue (455 nm) Lambertian operating at approximately 340 mW (700 mA). Relaxation rates at 20 °C were measured by recording the change in absorbance at 350 nm. Data were fitted to single-exponential functions to extract rate constants.

Urea Denaturation Studies. Protein samples (∼5 μM) were prepared in 1× TAE, 100 mM NaCl (pH 7.5) with 8 M urea. Fluorescence emission at 360 nm (excitation at 280 nm, 2 nm excitation and emission slits) was monitored as the solution was titrated with the same solution without urea using an AVIV (Lakewood, NJ) ATF-105 automatic titrating fluorometer. Data were recorded at 1 min intervals with stirring upon each addition. Fluorescence refolding curves were obtained at 20 and 30 °C.

Scheme 1: Primary Sequence of the GCN4Δ25PYP-v2 Protein[a]

[a]Purple for a GCN4 residue, yellow for a PYP residue, cyan for a residue chosen by Rosetta, and red for the vector-encoded His tag (residues 34−58 being the N-terminal cap).

Fluorescence data were then fitted using the equation

$$F_{360} = \frac{\alpha_N + \beta_N[\text{urea}] + \alpha_D + \beta_D[\text{urea}]\exp[m_{D-N}([\text{urea}] - [D]^{50\%})/RT]}{1 + \exp[m_{D-N}([\text{urea}] - [D]^{50\%})/RT]} \quad (1)$$

where α_N is F_{360} in the absence of urea, β_N is the slope (F_{360} vs [urea]) at the beginning of the curve, α_D is the value of F_{360} for the fully denatured state, and β_D is the slope at the end of the transition. The quantity $[D]^{50\%}$ is the urea concentration at the point where the protein is 50% unfolded, and the term m_{D-N} is a proportionality constant that reflects the degree of unfolding of the protein in urea (*13*). Differential values for the free energies of folding of mutants versus GCN4Δ25PYP-v2 protein at the midpoint urea concentration were obtained from the equations $\Delta\Delta G([D]^{50\%}) = 0.5(m_{D-N} + m'_{D-N})\Delta([D]^{50\%})$ and $\Delta\Delta G(H_2O) = m_{D-N}([D]^{50\%}) - m'_{D-N}([D]^{50\%\prime})$ (*14*), where the term m'_{D-N} refers to the mutant.

DNA Binding Assays. All samples for the electrophoretic mobility shift assay were prepared under red light. To 20 mM Tris-HCl (pH 7.5), 100 mM KCl, 3 mM $MgCl_2$, 0.1% Triton, 5% glycerol, 100 μg/mL BSA, and 1 mg/mL sheared salmon testes DNA were added 10 nM annealed Cy-3-labeled AP-1 DNA and the GCN4Δ25PYP-v2 mutant protein at final concentrations of 1 nM, 5 nM, 10 nM, 25 nM, 50 nM, 75 nM, 100 nM, 125 nM, 250 nM, 375 nM, 500 nM, 750 nM, 1 μM, and 3 μM in a total volume of 100 μL. Samples were incubated overnight in the dark at 4 or 20 °C. The following day, 20 μL of the sample was run in the dark on an 8% native polyacrylamide gel containing 1× TAE buffer (pH 7.5) that is also used as the running buffer. Gels were run at 4 °C for 105 min at 300 V using an Emperor Penguin Water cooled dual-gel electrophoresis system. The gel was scanned with a green laser (532 nm) on a GE Healthcare Typhoon 9400 instrument. The remaining samples were irradiated with a Luxeon III Star LED Royal Blue instrument (455 nm) for 5 min, and then another 20 μL aliquot was loaded onto another 8% native polyacryamide gel prepared as described above. The gel was run and imaged as described above except that two Luxeon III Star LED Royal Blue instruments (455 nm) each at 340 mW (700 mA) were irradiating the gel continuously during the run. Heat from the LEDs was dissipated by the temperature-regulated gel tank buffer. To determine the reversibility of DNA binding, the remaining samples were incubated in the dark overnight, and then a 20 μL aliquot was run on another 8% native polyacrylamide gel prepared as described above. The gel was run in the dark and imaged as detailed above. DNA binding was quantified by analysis with ImageQuant version 5.0. Using IgorPro, each set of data was fit to the Hill equation to determine apparent K_d values, the concentration of protein required for half-maximal binding to the AP-1 site, and Hill coefficients. Hill coefficients were found to vary between 1.6 and 2.6 when left unconstrained in the fitting. Hill coefficients were then constrained to 2 and apparent K_d values recalculated. The average and standard deviation from fits of experiments performed in triplicate are reported.

RESULTS

Mutational Design. In designing a GCN4Δ25PYP hybrid, we intended to choose a GCN4 segment that could pack against the PYP core (residues 59−157) in the dark-adapted state in a manner that sterically impedes the ability of the coiled-coil domain to dimerize (*8*). When irradiated, this N-terminal cap region (residues 34−58) is expected to disengage from the PYP core and expose the coiled-coil sequence leading to dimerization and DNA binding. The amino acid sequence of GCN4Δ25PYP-v2 is shown in Scheme 1.

To improve the degree of switching of DNA binding, we attempted to decrease the affinity for DNA in the dark while maintaining or enhancing it in the light. It is useful to consider what classes of mutation might be expected. For instance, one could alter residues in GCN4Δ25PYP-v2 that comprise part of the basic DNA binding region (residues 8−23). Because this region is not expected to interact with the PYP domain in the light or the dark, mutations would be expected to affect light and dark GCN4Δ25PYP-v2 DNA affinity equally, i.e., have no effect on the degree of switching. Similarly, changes to residues that comprise part of the PYP core but that do not interact with the N-terminal cap would not be expected to alter DNA binding in the light or dark unless they substantially altered the overall light-driven conformational change. Therefore, we focused on residues that form part of the N-terminal cap (residues 34−58). These are expected to interact with the PYP core (residues 59−157) in the dark but interact with another N-terminal cap (to form a coiled coil) when irradiated. In addition, residues in the PYP core domain that interact with the N-terminal cap in the dark may help to stabilize the dark state (and thereby decrease DNA binding affinity in the dark) but have no direct effect on the coiled-coil structure.

Using the modeled structure of the PYP domain of GCN4Δ25PYP-v2 (*8*), which is based on the high-resolution X-ray structure of wild-type PYP [Protein Data Bank (PDB) entry 1NWZ] (*15*), we used PoPMuSiC 2.0 (http://babylone.ulb.ac.be/popmusic) to identify residues for which the stability of the dark-state protein might be enhanced. This program uses statistical potentials that combine four distinct protein sequence and structure descriptors and takes into account amino acid volume variation upon mutation. The calculated stability change also depends on the calculated solvent accessibility of the mutated residue. The key feature of PoPMuSiC 2.0, in addition to its superior performance in tests against experimental data, is its ability to rapidly predict the stability changes resulting from all possible mutations in a protein (*16*, *17*). Using the PoPMuSiC 2.0 algorithm, sites predicted to be most likely to lead to enhanced protein stability were identified. These are collected in Table 1 together with the mutations that are predicted to be stabilizing.

Table 1: Sites and Mutations Predicted To Enhance GCN4Δ25PYP-v2 Stability by PoPMuSiC 2.0[a]

residue in GCN4Δ25PYP-v2	stabilizing mutations
E35	F (−1.60), L (−1.54), I (−1.52), W (−1.34), Y (−1.30), M (−1.21), V (−1.10), H (−0.61), Q (−0.29), R (−0.20), T (−0.33)
E45	I (−0.71), V (−0.43), F (−0.41), L (−0.35), M (−0.32), Y (−0.21)
G54	A (−0.44), E (−0.36), D (−0.32), S (−0.30)
Q65	I (−0.86), L (−0.50), V (−0.46), M (−0.46), F (−0.44), W (−0.42), Y (0.40), H (−0.30)
R85	I (−0.60), L (−0.58), W (−0.40), Y (−0.37), V (−0.30), M (−0.27), F (−0.22)
K143	F (−1.02), L (−0.76), Y (−0.66), I (−0.64), W (−0.64), V (−0.59), M (−0.44), H (−0.14)
K144	L (−0.72), W (−0.63), F (−0.51), M (−0.46), I (−0.45), Y (−0.36), V (−0.27), P (−0.11)

[a]Numbers in parentheses are the calculated differences in dark-state (pG) folded stability in kilocalories per mole.

Table 2: Calculated Stabilities of Single-Point Mutants of the Coiled-Coil-Forming Domain of GCN4Δ25PYP-v2[a]

GCN4Δ25PYP-v2 numbering	27	28	29	30	31	32	33	34	35	36	37	38	39	40	41	42	43	44	45	46	47	48	49	50	51	52	53	54	55	56	57	58
heptad position	*a*	*b*	*c*	*d*	*e*	*f*	*g*	*a*	*b*	*c*	*d*	*e*	*f*	*g*	*a*	*b*	*c*	*d*	*e*	*f*	*g*	*a*	*b*	*c*	*d*	*e*	*f*	*g*	*a*	*b*	*c*	*d*
GCN4Δ25PYP-v2 sequence	M	K	Q	L	E	D	K	V	E	E	L	A	F	G	N	E	H	L	E	E	E	L	A	R	L	K	K	G	Q	L	D	R
A								26	24	24		27	30	38	28	24	31		24	24	12		27	29		16	29	38	34	27	32	35
D								15	19	19		26	25	25	18	19	26		19	19	11		22	24		2	24	33	23	22	27	24
E								22	***27***	***27***		***42***	***32***	32	25	***27***	***33***		***27***	***27***	***27***		***29***	***31***		9	***31***	***40***	30	***30***	***34***	31
F								17	21	21		24	27	35	20	21	28		21	21	9		24	26		13	26	35	25	24	29	26
G								8	13	13		15	18	27	11	13	19		13	13	0		15	17		4	17	27	17	16	20	17
H								16	20	20		22	25	34	18	20	27		20	20	7		22	25		12	24	34	24	23	27	25
I								28	21	21		23	26	34	31	21	27	18	21	21	8		23	25		12	25	34	36	24	28	37
K								18	22	22		16	27	***49***	20	22	29		22	22	1		24	27		***27***	27	36	26	25	29	27
L								***37***	24	24	27	26	29	37	***39***	24	30	27	24	24	11	27	26	28	27	15	28	37	***45***	27	31	***46***
M								19	23	23		25	28	37	21	23	30		23	23	10		25	28	8	15	27	37	27	26	30	28
N								24	17	17		19	22	31	27	17	23		17	17	4		19	21		8	21	31	32	20	24	33
Q								18	23	23		34	28	41	21	23	29		23	23	19		25	27		18	27	37	27	26	30	27
R								18	22	22		16	27	***49***	20	22	28		22	22	1		24	27		26	26	36	26	25	29	27
S								10	14	14		17	20	28	13	14	21		14	14	2		17	19		6	19	28	18	17	22	19
T								12	17	17		19	22	31	15	17	23		17	17	4		19	21		8	21	31	21	20	24	21
V								27	19	19	16	21	24	33	29	19	26		19	19	6	16	21	24		11	24	33	35	22	26	36
W								15	20	20		22	25	34	18	20	26		20	20	7		22	24		11	24	34	24	23	27	24
Y								12	17	17		19	22	30	15	17	23		17	17	4		19	21		8	21	30	20	19	24	21
wt GCN4 numbering	2	3	4	5	6	7	8	9	10	11	12	13	14	15	16	17	18	19	20	21	22	23	24	25	26	27	28	29	30	31	32	33
wt PYP numbering								1	2	3	4	5	6	7	8	9	10	11	12	13	14	15	16	17	18	19	20	21	22	23	24	25

XX most stabilizing mutation | GCN4 residue | PYP residue | mutation target | Rosetta mutation

[a]Heptad positions that can make electrostatic interactions (*g*,*e*) are indicated with the same color. Only a limited number of mutations were considered at *a* and *d* (core hydrophobic) positions. Proline and cysteine substitutions were not considered.

Of these sites, E35, E45, and G54 are all part of the N-terminal cap while K143 and K144 are part of the PYP core domain that interacts with the N-terminal cap. In contrast, Q65 and R85 do not appear to interact with the N-terminal cap and were therefore excluded.

Any changes made to the N-terminal cap sequence must also be considered in terms of their potential effects on the formation of coiled coils, the intended light-adapted state. To assess the effects of mutations on the formation of coiled coils, we used the algorithm for predicting coiled-coil stability developed by Arndt and colleagues (bCIPA, http://www.molbiotech.uni-freiburg.de/bCIPA/). Coiled coils are characterized by a heptad repeat sequence, *abcdefg*, where positions *a* and *d* form the hydrophobic dimerization interface and are particularly important for stability. In addition, the Asn residue that occurs at an *a* position in GCN4 [N16 in the wild-type (wt) sequence] is known to promote the formation of parallel, dimeric, coiled-coil structures and disfavor the formation of higher-order coils (*18*). Mutations at this position and at positions *a* and *d* were avoided. Table 2 lists all the options examined and their expected melting temperatures. The higher the melting temperature, the more stabilizing the mutation.

Residues identified as stabilizing by the PoPMuSiC 2.0 algorithm at position E35 include the hydrophobic residues F, L, I, W, Y, M, and V. Of these, none are stabilizing with respect to the formation of coiled coils; the least detrimental are L and M. At the E45 site, again PoPMuSiC 2.0 suggests hydrophobic residues (I, V, F, L, M, and Y). This site is an *e* position of the heptad and therefore can interact with the preceding *g* position of the other monomer in the coiled coil (Table 2). Often in coiled coils such $e-g'$ interactions are electrostatic in nature (*20*). However, in this case, a glycine residue was introduced at the preceding *g* position (*8*) because this residue in PYP adopts torsion angles available to only Gly in the Ramachandran plot and is partially conserved (*21*). While the Glu residue (the GCN4Δ25PYP-v2 residue) is the most stabilizing at position 45, a variety of other residues are compatible with the formation of coiled coils with relatively minor negative effects on stability (Table 2). The

PoPMuSiC 2.0 algorithm predicts that the G54 site may be mutated to A, E, D, or S with an increase in stability. The bCIPA algorithm predicts that any of these mutations, in particular G54E and G54A, will also enhance coiled-coil stability.

The other two residues suggested by PoPMuSiC 2.0 as sites for enhancing stability were K143 and K144. These are sites that are part of the PYP core domain, so changes to either of these residues are not expected to affect coiled-coil stability in the light state. However, both residues can interact with the N-terminal cap (residues 34−58), with K143 making closer contact with the cap than K144. K143 is in the proximity of E45; in fact, these residues make a salt bridge in the X-ray crystal structure (E12−K110 in wild-type numbering) that has been proposed to be important for N-terminal cap stability (*22*). As a result, changes to residues E45, K143, and K144 are likely to be interdependent.

We explored interdependent mutations of the group of residues E35, E45, G54, K143, and K144 using the Rosetta design algorithm (*23*) as well as the Eris protein stability prediction server (http://troll.med.unc.edu/eris/login.php) (*24*, *25*). The Rosetta design algorithm was used previously in the design of GCN4Δ25PYP-v2 (*8*). Rather than using Rosetta for extensive redesign, we focused on generating mutations at the E35, E45, G54, K143, and K144 sites to search for optimal combinations of changes. Rosetta predicted the largest stability improvement would occur with E35 changed to either A or M (E35A or E35M, respectively), G54 changed to E (G54E), E45 changed to K together with K143 changed to I (E45K/K143I), and K144 unchanged. The Eris server calculates the change in protein stability induced by mutations utilizing the Medusa modeling suite. Whereas the Rosetta approach used a fixed backbone, the Eris server permits backbone flexibility. The Eris server returned E35A as preferable to E35M, and G54E and G54A as equally stabilizing. Mutation to hydrophobic residues was predicted to be particularly stabilizing at K143, more so than at K144. Additionally, if K143 was mutated to a hydrophobic residue, both the Eris server and the PoPMuSiC 2.0 algorithm indicated that further mutation of K144 to a hydrophobic residue would not lead to further stabilization. Because we also wanted to avoid the creation of hydrophobic patches on the protein surface that may lead to lower solubility and possible aggregation, we opted to focus hydrophobic mutation at position K143. The following mutations were ultimately chosen: G54A, G54E, K143I, K143F, G54E/K143I, E35M/G54E/K143I, E35M/G54E/K143F, E45K/G54E/K143I, and E35M/E45K/G54E/K143I. These are highlighted in orange in Table 2 and Figures 1 and 2.

Protein Expression, Purification, and Preliminary Characterization. Single-point mutations in GCN4Δ25PYP-v2 were introduced using the Stratagene Quikchange protocol (Agilent, Inc.) and confirmed by automated DNA sequencing (ACGT Corp, Toronto, ON). Each of the mutants was expressed in *Escherichia coli* BL21cells; the 4-hydroxycinnamic acid chromophore, activated as a thioester (*12*), was added during expression. All mutants were expressed well, purified by immobilized metal affinity chromatography, and analyzed by electrospray mass spectrometry. The masses observed were consistent with >95% holoprotein without any N-terminal processing. All proteins gave dark-adapted absorbance spectra similar to that of GCN4Δ25PYP-v2 (Figure 3). The wavelengths of the absorbance maxima are all close to 446 ± 2 nm, similar to that of wild-type PYP (*26*). Absorbance ratios (A_{446}/A_{280}) were generally

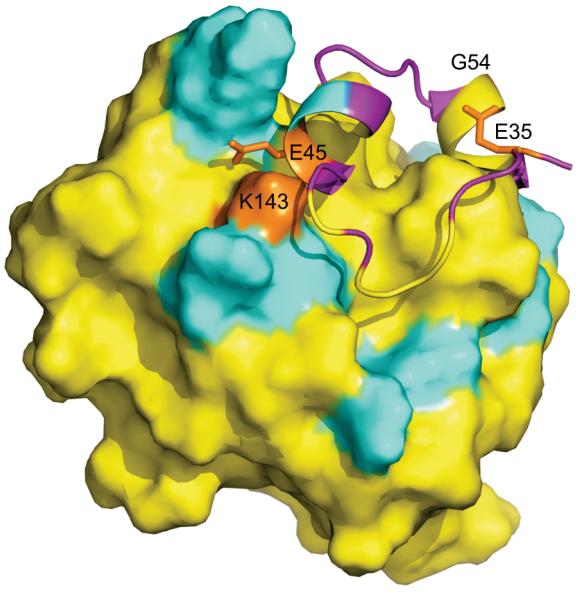

FIGURE 1: Sequence of GCN4Δ25PYP-v2 modeled onto the structure of wild-type PYP (Protein Data Bank entry 1NWZ) (*15*). Residues 59−157 (the "core" domain) of PYP are shown as a solid surface. Residues that are part of GCN4 or the N-terminal cap (34−58) are shown as a ribbon. Colors follow the convention of Scheme 1 (yellow for PYP residues, purple for GCN4 residues, and cyan for residues changed in the hybrid that are not PYP or GCN4 residues). The unstructured basic region sequence of GCN4 is truncated for the sake of clarity. Residues targeted for mutagenesis in this study are colored orange and labeled.

near 2.0, consistent with >95% holoprotein (*26*). Some variation in this ratio may be due to effects of mutations on absorbance coefficients. The presence of apoprotein would be expected to decrease the degree of photoswitching of DNA binding observed because apoprotein would bind DNA with the same affinity whether dark-adapted or irradiated.

Stability of the Dark-Adapted State: Urea Denaturation. To assess the effects of mutation on the stability of dark-state GCN4Δ25PYP-v2 mutants, urea denaturation experiments were performed by measuring the fluorescence emission at 360 nm (excitation at 280 nm) as a function of urea concentration. A temperature of 30 °C was used so that complete denaturation of the most stable mutants was observed. Similar relative stabilities among mutants were observed at 20 °C. Figure 4 shows the urea denaturation curves measured for the mutants together with those for GCN4Δ25PYP-v2, wild-type PYP, and Δ25PYP. The denaturation midpoints together with estimated $\Delta\Delta G$ values for folding (assuming a simple two-state model) (*13*) are listed in Table 3.

Clearly, some of the designed mutations have indeed stabilized the dark-adapted protein compared to GCN4Δ25PYP-v2. It appears that hydrophobic mutations at K143 are particularly effective as predicted by the PoPMuSiC 2.0 algorithm.

Effects of DNA Addition: Thermal Relaxation Rates Monitored Using UV−Vis Methods. To probe the interaction of the mutants with AP-1 DNA, we measured the thermal relaxation of the constructs by monitoring the decay of absorbance at 350 nm (pB form) as a function of time in the presence and absence of nonspecific and specific (AP-1) DNA. These data are listed in Table 4. Rate constants derived from fitting to either a single-exponential process or double-exponential process were obtained. Lee and Hoff have suggested that double-exponential decays in PYP may arise from formation

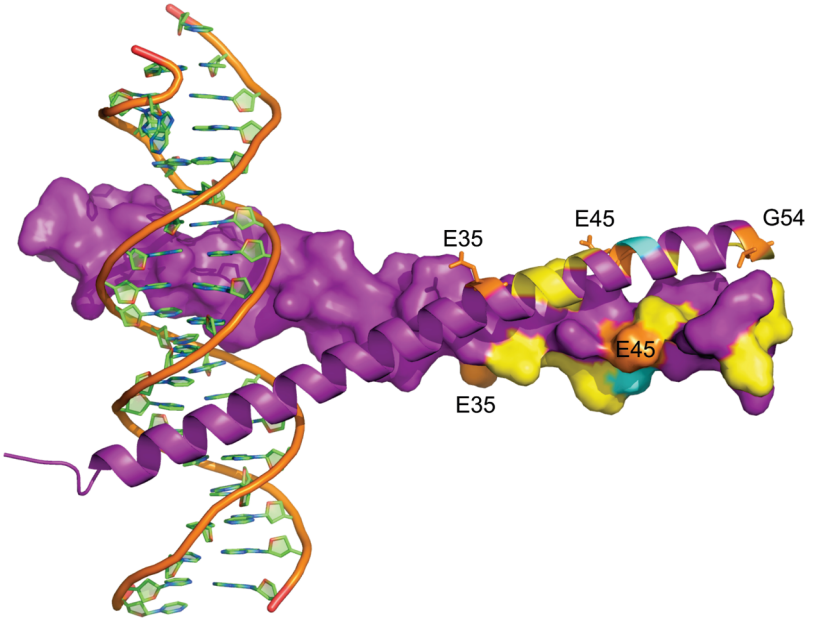

FIGURE 2: Sequence of GCN4Δ25PYP-v2 modeled onto the structure of wt GCN4 bound to DNA as a dimer (PDB entry 1YSA) (*19*), the intended light-adapted state. Residues 59−157 of the PYP domain have been omitted for the sake of clarity. One monomer is shown as a ribbon and the other as a solid surface. Colors follow the conventions of Scheme 1 (yellow for PYP residues, purple for GCN4 residues, and cyan for residues changed in the hybrid that are not PYP or GCN4 residues). Residues targeted for mutagenesis in this study are colored orange and labeled.

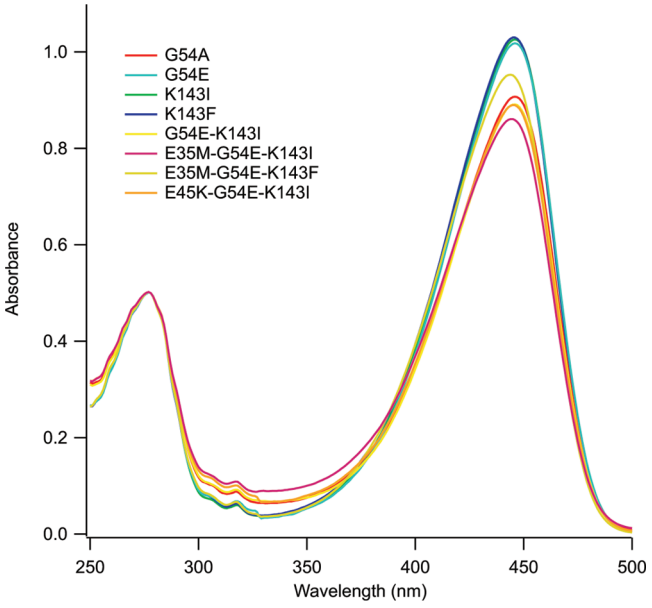

FIGURE 3: UV−vis spectra of a subset of GCN4Δ25PYP-v2 mutants in TAE (pH 7.5) and 100 mM NaCl at 4 °C. Protein concentrations were approximately 5 μM (absorbance normalized at 278 nm).

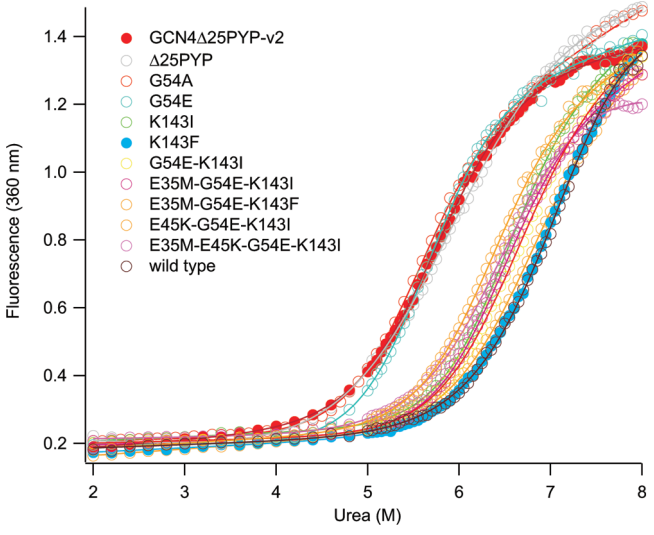

FIGURE 4: Urea denaturation of GCN4Δ25PYP-v2 mutants in TAE (pH 7.5) and 100 mM NaCl at 30 °C as monitored by measuring fluorescence emission at 360 nm (excitation at 280 nm). Protein concentrations were approximately 5 μM.

of a fraction of a *cis*-proline isomer upon irradiation that subsequently reverts to a *trans*-proline isomer (*27*). While fitting to double-exponential decays did provide better fits to the data in some cases, single-exponential fits also clearly reflected overall effects of DNA binding on thermal relaxation. At the protein and DNA concentrations tested, all the protein is expected to become DNA bound upon addition of AP-1 DNA whether the protein is irradiated or dark-adapted (see below).

The deletion of the N-terminal cap has previously been shown to slow the PYP photocycle (*28*, *29*). Although Δ25PYP does not bind DNA specifically, addition of nonspecific DNA slows the relaxation rate of Δ25PYP somewhat perhaps via interactions with the exposed hydrophobic surface of the protein. The relaxation rate of the pB form of GCN4Δ25PYP-v2, in contrast, is specifically slowed ~6-fold by binding to AP-1 DNA, whereas nonspecific DNA causes a slight acceleration. The mutants show a variety of effects; in some cases (e.g., E45K/G54E/K143I), nonspecific DNA has a pronounced slowing effect, with subsequent specific binding to AP-1 having a less dramatic effect. In other cases (e.g., K143F and G54E/K143I), nonspecific DNA has a minimal effect and AP-1 DNA has a marked effect, slowing relaxation almost 10-fold.

Photoswitchable DNA Binding Activity. We further assayed the ability of the mutants to specifically recognize the AP-1 sequence by performing electrophoretic mobility shift assays using Cy3-labeled AP-1 in the presence of excess nonspecific

Table 3: Calculated Midpoints ($[D]^{50\%}$) for Urea Denaturation of GCN4Δ25PYP-v2 Mutants in TAE (pH 7.5) and 100 mM NaCl at 30 °C[a]

protein	$[D]^{50\%}$ (M)	m_{D-N} (kcal/mol^2)	$\Delta\Delta G([D]^{50\%})$ (kcal/mol)	$\Delta\Delta G(H_2O)$ (kcal/mol)
GCN4Δ25PYP-v2	5.72 ± 0.01	1.29 ± 0.03	–	–
Δ25PYP	5.84 ± 0.03	0.99 ± 0.02	−0.20	1.6
G54A	5.46 ± 0.01	1.45 ± 0.04	0.54	−0.5
G54E	5.61 ± 0.02	1.51 ± 0.03	0.24	−1.1
K143I	6.43 ± 0.02	1.52 ± 0.03	−1.54	−2.4
K143F	6.88 ± 0.05	1.22 ± 0.02	−2.16	−1.0
G54E/K143I	6.53 ± 0.03	1.34 ± 0.03	−1.61	−1.4
E35M/G54E/K143I	6.40 ± 0.03	1.49 ± 0.04	−1.45	−2.1
E35M/G54E/K143F	6.71 ± 0.03	1.27 ± 0.02	−1.90	−1.1
E45K/G54E/K143I	6.30 ± 0.03	1.41 ± 0.04	−1.19	−1.5
E35M/E45K/G54E/K143I	6.53 ± 0.03	1.26 ± 0.03	−1.54	−0.9
wild type	7.20 ± 0.08	1.21 ± 0.03	−2.75	−1.3

[a]Values for m_{D-N} and free energies [$\Delta\Delta G([D]^{50\%})$ and $\Delta\Delta G(H_2O)$] were estimated as described in Materials and Methods.

Table 4: Lifetimes (seconds) for Thermal Relaxation of the pB (*cis*) Forms of the Proteins at 20 °C

protein	in TAE (pH 7.5) and 100 mM NaCl	with nonspecific DNA	with nonspecific DNA and equimolar AP-1 DNA	*n*-fold change (with AP-1)
GCN4Δ25PYP-v2	99 ± 3	80 ± 3	476 ± 20	5.9
Δ25PYP	212 ± 6	225 ± 5	225 ± 5	1
G54A	221 ± 6	150 ± 4	552 ± 20	3.7
G54E	137 ± 4	100 ± 3	349 ± 15	3.5
K143I	91 ± 3	87 ± 7	740 ± 20	8.5
K143F	96 ± 3	132 ± 3	1189 ± 60	9
G54E/K143I	54 ± 4	60 ± 5	565 ± 20	9.4
E35M/G54E/K143I	92 ± 4	122 ± 5	724 ± 20	5.9
E35M/G54E/K143F	68 ± 2	144 ± 4	771 ± 15	5.4
E45K/G54E/K143I	243 ± 5	684 ± 15	882 ± 20	1.3
E35M/E45K/G54E/K143I	215 ± 6	325 ± 15	700 ± 20	2.1

Table 5: Specific AP-1 DNA Apparent Binding Affinities of the Proteins in Dark-Adapted and Irradiated States

protein	apparent K_d dark-adapted (nM)	apparent K_d irradiated (nM)	apparent K_d(dark)/apparent K_d(light)	maximal *n*-fold increase in % DNA bound
GCN4Δ25PYP-v2	571 ± 17	297 ± 11	1.9	3.6
G54A	528 ± 16	356 ± 15	1.5	2.3
G54E	717 ± 15	392 ± 15	1.8	3.2
K143I	635 ± 15	264 ± 11	2.4	5.8
K143F	383 ± 13	108 ± 8	3.5	12
G54E/K143I	301 ± 15	119 ± 8	2.5	6.3
E35M/G54E/K143I	305 ± 16	166 ± 10	1.8	3.2
E35M/G54E/K143F	165 ± 6	74 ± 6	2.2	4.8
E45K/G54E/K143I	121 ± 10	120 ± 10	1.0	1.0
E35M/E45K/G54E/K143I	159 ± 11	134 ± 10	1.2	1.4

DNA. DNA binding affinities of the proteins in the dark-adapted state and irradiated state were calculated on the basis of the analysis of these gels and fitting to the Hill equation as described previously (*8*). Apparent affinities (the protein concentration required for half-maximal binding) are listed in Table 5, and sample data for the mutant showing the largest change in affinity upon irradiation (K143F) are shown in Figure 5. All binding was reversible.

The parent protein GCN4Δ25PYP-v2 shows an enhanced affinity for AP-1 when irradiated. The observed 2-fold decrease in the apparent K_d (from 571 ± 17 to 297 ± 11 nM), while small, is reproducible and reversible after dark adaptation. All of the mutants studied also showed enhanced DNA binding upon irradiation. In some cases (e.g., E45K/G54E/K143I), this was minimal, whereas in others (e.g., K143F and G54E/K143I), this was significantly enhanced compared to the parent. In addition, the dark-adapted DNA binding affinity varied considerably. In some cases, it was similar to or weaker than that of GCN4Δ25PYP-v2, but in many cases, it was significantly tighter. In some cases (e.g., E45K/G54E/K143I), it approached that of free wild-type GCN4 without PYP (*30*)(apparent $K_d \sim 60$ nM). Hill coefficients derived from fitted binding curves varied between 1.6 and 2.6, suggesting the proteins dimerize upon binding to DNA, which occurs for native GCN4 (*30*). Constraining the Hill coefficients to 2 gave apparent K_d values similar to those obtained using unconstrained fits. Forcing the Hill coefficient to be 1 gave very poor fits.

Further Characterization of the K143F Mutant. Because the GCN4Δ25PYP-v2 K143F mutant had the largest effect of irradiation on specific AP-1 DNA binding as well as the largest increase in dark-state stability, we characterized that mutant

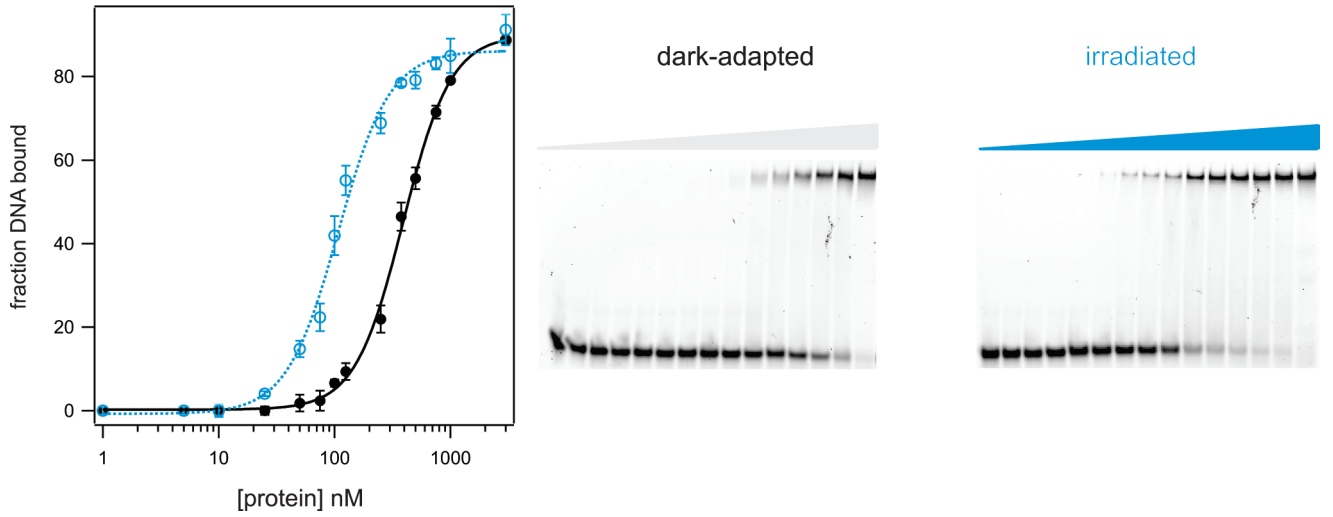

FIGURE 5: EMSA of the GCN4Δ25PYP-v2 K143F mutant with AP-1 target DNA. Binding buffer consisted of 20 mM Tris (pH 7.5), 100 mM KCl, 3 mM $MgCl_2$, 0.1% Triton, 5% glycerol, 100 μg/mL BSA, and 1 mg/mL salmon testes DNA. The concentration of 5′-Cy-3-labeled AP-1 DNA was 10 nM. Running buffer was TAE buffer (pH 7.5). Gels were run either in the dark or under constant 460 nm LED illumination at 4 °C. Protein concentrations on gel images shown are 0, 1, 5,10, 25, 50, 75, 100, 125, 250, 375, 500, 750, 1000, and 3000 nM.

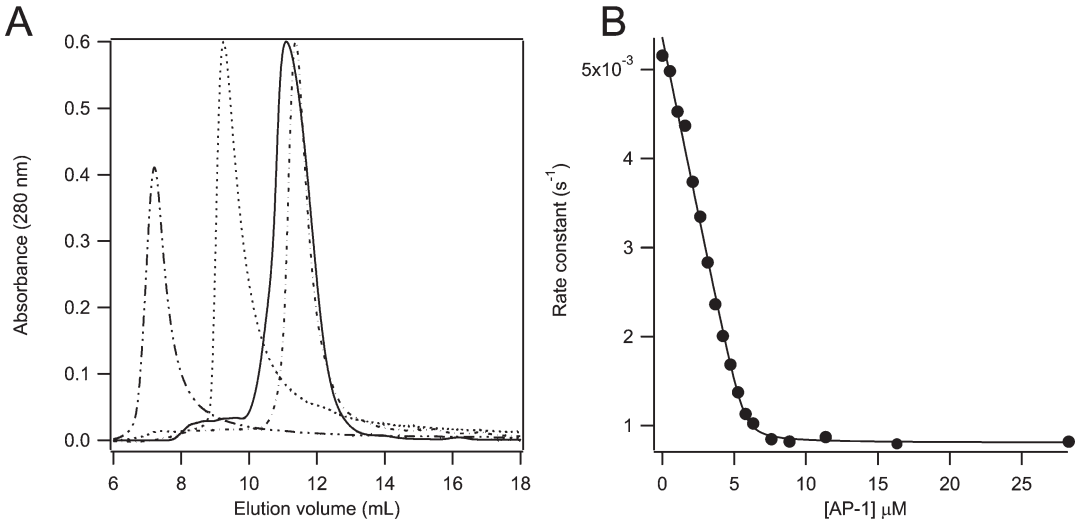

FIGURE 6: (A) Size exclusion (G75) chromatography of dark-adapted GCN4Δ25PYP-v2 K143F (—) in TAE buffer (pH 7.5) and 100 mM NaCl. GCN4PYP (---) is dimeric (44790 Da) and GCN4Δ25PYP-v2 (−-−) monomeric (19644 Da) under these conditions (*8*). The elution pattern of blue dextran (−···−) indicates the void volume of the column. (B) Rate constants calculated from exponential fits to pB thermal relaxation data (absorbance at 350 nm) for 10 μM GCN4Δ25PYP-v2 K143F in the absence of AP-1 DNA and with increasing amounts of AP-1 DNA in TAE buffer (pH 7.5) and 100 mM NaCl, at 20 °C, with 1 mg/mL salmon testes DNA.

further to confirm its molecularity in the dark-adapted state in the absence of DNA as well as its DNA binding stoichiometry.

Size exclusion chromatography analysis confirmed that GCN4Δ25PYP-v2 K143F behaved as a monomer in the dark (Figure 6A). Its elution volume matched that of GCN4Δ25PYP-v2 and was much larger than that of previously reported GCN4-PYP for which equilibrium analytical ultracentrifugation analysis yielded monomer and dimer masses, respectively (*8*).

Measurement of the thermal relaxation rate of the pB form of the protein as a function of the concentration of AP-1 DNA (Figure 6B) confirmed that GCN4Δ25PYP-v2 K143F bound DNA as a dimer. No further slowing of the relaxation rate was observed after a mole ratio of 1:2 (DNA:protein) was reached.

DISCUSSION

Our intent in this work was to increase the degree of photoswitchable specific AP-1 DNA binding by the designed chimeric protein GCN4Δ25PYP-v2. Strickland et al. (*7*) have pointed out that fusion of a switchable protein to an intended effector domain is likely to alter the on−off balance of the switchable domain. In the case of the LOV photoswitchable domain fused to the Trp repressor, packing of the J-α helix against the LOV domain is intended in the dark. In their original design, fusion to the Trp repressor appears to destabilize the packing of the helix so that when the LOV domain is irradiated, only a small extra degree of disengagement of the J-α helix is possible; hence, the degree of photoswitching is small. By stabilizing the helix packing against the LOV domain in the dark state of the chimera with a few carefully chosen mutations, these authors were able to increase the degree of photoswitching substantially (*7*).

In the case presented here, we were seeking to pack the dimerizing coiled-coil domain of GCN4 against the PYP core in the dark, thereby diminishing its DNA binding ability. At the same time, we wished to preserve high-affinity specific DNA

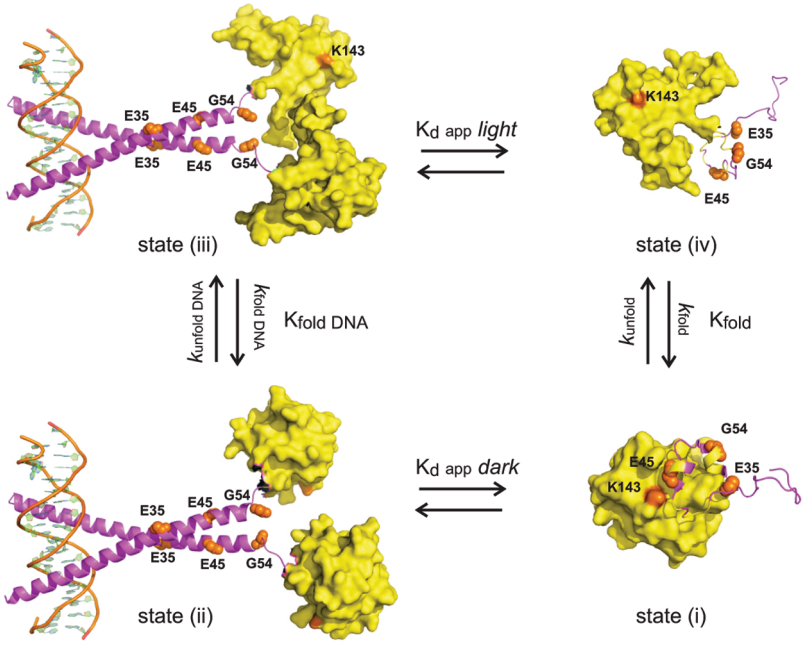

FIGURE 7: Thermodynamic cycle describing DNA binding by GCN4Δ25PYP fusion proteins. All structures are models only. Coloring is the same as in Figures 1 and 2 except cyan has been omitted for the sake of clarity. GCN4 residues are colored purple and PYP residues yellow. Mutated sites are shown as orange space fill. Surfaces represent the core of PYP (residues 59−157). State i is the folded dark-state structure based on wild-type PYP (PDB entry 1NWZ). State ii retains the dark-state fold of the PYP core, but the N-cap residues are unpacked from the PYP core and participate in formation of a coiled coil. The coiled coil is based on wild-type bZIP GCN4 bound to DNA (PDB entry 1YSA) (*19*). State iii is the same as state ii except that the PYP core is partially unfolded. One structure from the NMR-derived ensemble of structures for light-adapted Δ25PYP is shown (PDB entry 1XFQ) (*29*). State iv is the partially unfolded core of PYP with the N-cap detached.

binding in the irradiated state. As a framework for considering the results obtained, it is useful to view the system as the thermodynamic cycle shown in Figure 7. Four states are identified: (i) a folded PYP domain (pG) with the GCN4 zipper domain packed against the PYP core, (ii) a folded PYP domain (pG) with the GCN4 zipper domain dimerized and bound to DNA, (iii) a partially unfolded PYP domain (pB) with the GCN4 zipper domain dimerized and bound to DNA, and (iv) a partially unfolded PYP domain (pB) with the GCN4 zipper domain free. Shining blue light on the system may be regarded as perturbing it in a manner that produces pB states (iii and iv) at the expense of pG states (i and ii). In the dark, these four states are connected in a thermodynamic cycle (Figure 7) in which

$$K_{d,app}(\text{light})K_{fold} = K_{d,app}(\text{dark})K_{foldDNA} \quad (2)$$

As in the LOV/Trp repressor case, we anticipated that introducing mutations that would stabilize the packing of the N-cap upon the PYP core would enhance photoswitching, if they would selectively stabilize state i and have no effect on states ii−iv. Our approach to choosing the mutations is described in detail above. The following mutations were ultimately chosen: G54A, G54E, K143I, K143F, G54E/K143I, E35M/G54E/K143I, E35M/G54E/K143F, E45K/G54E/K143I, and E35M/E45K/G54E/K143I. These sites are highlighted in orange in Table 2 and Figures 1, 2, and 7. All mutant proteins were expressed and purified, gave UV−vis spectra like that of the parent protein GCN4Δ25PYP-v2, and underwent normal photocycles.

Urea denaturation studies were first performed to gauge the effects of mutations on dark-state stability of the proteins. Whereas wild-type PYP has a urea denaturation midpoint ($[D]^{50\%}$) of 7.2 M (*31*), Δ25PYP, the protein missing the N-terminal cap entirely, has a $[D]^{50\%}$ of 5.9 M (Table 3). This result indicates that substantial stabilization is available from an N-terminal cap that is well packed onto the PYP core. The parent hybrid protein GCN4Δ25PYP-v2 has a urea midpoint slightly lower than that of Δ25PYP, indicating that the N-terminal cap in that case contributes nothing to protein stabilization. Although CD and fluorescence data indicate the cap is packed against the core in GCN4Δ25PYP-v2 (*8*), it may be only loosely packed so that no overall stabilization is obtained.

Changes at position K143 to hydrophobic residues were predicted by PoPMuSiC 2.0 to be particularly stabilizing (Table 1). Experimentally, we found this to be the case. Both K143I and K143F mutations were significantly stabilizing. The K143F mutation increased the $[D]^{50\%}$ value to 6.9 M, which corresponds to an increase in stability of ~2.2 kcal/mol relative to that of GCN4Δ25PYP-v2 (*14*). Mutations at sites E35 and E45 that are part of the segment forming the coiled coil produced only small enhancements in stability. In contrast, G54A and G54E mutants proved to have almost no effect on stability.

The DNA binding abilities of these mutants were analyzed using electrophoretic mobility shift assays. There was no clear relationship between dark-state stability as judged by urea denaturation experiments and specific AP-1 DNA affinity in the dark-adapted state. Whereas the K143I and K143F mutants are both significantly more stable than GCN4Δ25PYP-v2, K143I has decreased dark-state AP-1 DNA binding affinity, while that of K143F was enhanced. The E35M/G54E/K143F and E45K/G54E/K143I mutants had enhanced stability and also enhanced dark-state DNA binding affinity.

When the proteins were irradiated, DNA binding affinity was enhanced in all cases, consistent with enhanced exposure of the residues forming coiled coils created by light-driven detachment of the N-cap from the PYP core. However, rather than being

silent in terms of light-state AP-1 DNA binding affinity, the set of mutations has a variety of effects, both weakening it (G54A and G54E) and enhancing it (e.g., K143F and E35M/G54E/K143F).

The thermodynamic cycle diagrammed in Figure 7 requires that, however the mutations are affecting the stability of states i−iv, there should be a relationship between the degree of photoswitching [$K_{d,app}$(dark)/$K_{d,app}$(light)] and the equilibrium constant for folding in the presence and absence of DNA (eq 2). In the dark, the pG (folded) state is substantially more stable than the pB state, so that at equilibrium, only the pG state is observed, making direct determination of K_{fold} and $K_{foldDNA}$ difficult. However, we measured the folding rate (Table 4), i.e., the rate of the thermal pB to pG transition in the PYP photocycle, in the presence or absence of DNA (i.e., k_{fold} and $k_{foldDNA}$ in Figure 7). As noted above, at the protein and DNA concentrations employed for UV−vis absorbance measurements, the protein will be completely bound to AP-1 DNA in both the dark-adapted and irradiated state.

Although only the ratio of the equilibrium constants for folding, not the rate constants, is constrained by the thermodynamic cycle, there appears to be an approximately linear relationship between the ratio of these rate constants (Table 4) and the degree of photoswitching (Table 5) as shown in Figure 8. In general, those mutants with a larger degree of photoswitching also have a slower refolding rate in the presence of DNA. That this relationship exists implies that the mutations are not substantially affecting the relative unfolding rates (k_{unfold} vs $k_{unfoldDNA}$).

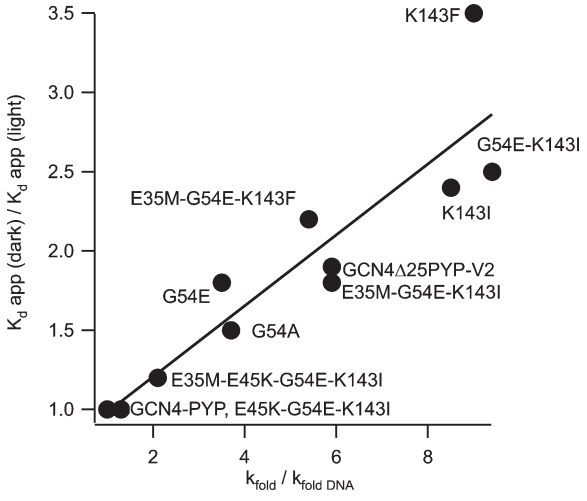

FIGURE 8: Observed relationship between the degree of photoswitching of AP-1 DNA binding [$K_{d,app}$(dark)/$K_{d,app}$(light)] and the ratio of k_{fold} to $k_{foldDNA}$ (see Figure 7).

Overall, these results indicate that, given a well-defined folded structure, computational tools, particularly PoPMuSiC 2.0, can rapidly identify sites such as position 143 where mutations can have significant stabilizing effects. However, our assumption that a more stable dark-state structure would lead to a greater degree of photoswitching was clearly too simplistic. First, it may be that the stabilization of the dark state, as judged by urea denaturation assays, does not directly reflect better packing of the N-cap domain on the PYP core; instead, resistance to denaturation is perhaps achieved by other means. Alternatively, or in addition, it may be that the mutations are affecting the stability of states other than state i in Figure 7. This conclusion is supported by the finding that mutations are affecting refolding rates (k_{fold} and $k_{foldDNA}$), a result that would not be expected if only changes in the stability of state i were involved. Structural studies aimed at elucidating features of states ii−iv may therefore help guide further improvements in photoswitch design.

Mutant K143F, which exhibited the largest degree of photoswitching (Table 5 and Figure 5) with an almost 4-fold decrease in the apparent K_d for AP-1 binding upon irradiation, also (together with G54E and K143I) was the mutant for which AP-1 DNA binding had the largest effect on the photocycle kinetics (Figure 8). The K143F mutant was also the most stable as judged by the urea denaturation assay (Table 3 and Figure 4). Further analysis of the GCN4Δ25PYP-v2 mutant by size exclusion chromatography showed that it behaved as a monomer in the dark (Figure 6A). The relaxation rate of the pB state was found to slow as the concentration of AP-1 DNA increased until a mole ratio of one AP-1 DNA duplex to two GCN4Δ25PYP-v2 K143F proteins was reached (Figure 6B). This result confirms that GCN4Δ25PYP-v2 K143F binds its target as a dimer, as designed. Overall, the K143F mutant seems well-behaved and a distinct improvement over the parent GCN4Δ25PYP-v2.

Although larger changes in DNA affinity are desirable before GCN4Δ25PYP proteins may be used as robust tools for photocontrol of transcription, if the K143F switchable protein were

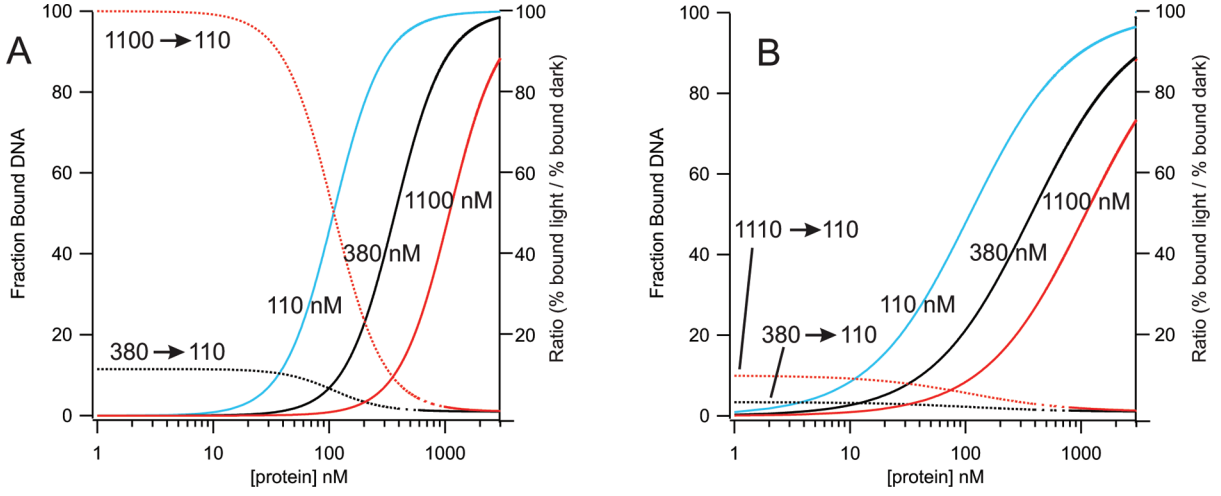

FIGURE 9: Calculated percentage of bound DNA (solid curves, left ordinate) assuming (A) cooperative binding (Hill coefficient of 2) or (B) noncooperative binding. Apparent K_d values are 110 (blue), 380 (black), and 1100 nM (red). Dotted curves are the calculated ratio of the percentage of bound DNA in the light to the percentage of bound DNA in the dark. Dotted curves use the right ordinate.

expressed at an ideal concentration, a ~12 fold-change in fraction DNA bound is possible because of the cooperativity of DNA binding by coiled-coil proteins (the Hill coefficients for all mutants were near 2.0). Figure 9 shows binding curves for K143F with the observed apparent K_d (i.e., half-maximal binding of 110 nM in the light and 380 nM in the dark). For the sake of simplicity, we assume the full range (0−100%) of binding occurs, whereas experimentally, a maximum of ~90% fraction bound DNA is observed likely because a small fraction of DNA is misfolded. Irradiation causes a decrease in the apparent K_d and so an increase in the fraction bound DNA for a given concentration of protein. The increase is plotted as a ratio (fraction bound DNA when irradiated/fraction bound DNA dark-adapted) as a function of protein concentration. The greatest increase in the fraction bound DNA occurs at lower protein concentrations. For instance, at 40 nM K143F, irradiation would cause an increase in the fraction bound DNA from 1 to 12% (12-fold). If there were no cooperativity, the maximal increase would be only 3.5-fold (Figure 9B). If further mutagenesis of GCN4Δ25PYP were to produce a protein that exhibited a 10-fold difference in the apparent K_d between dark and irradiated states (e.g., the apparent K_d of the dark-adapted protein was 1100 nM), a 100-fold change in the fraction bound DNA would be possible (Figure 9A). Note also that increasing the difference in the apparent K_d between dark and irradiated states leads to a wider range of protein concentrations over which substantial increases in the fraction DNA bound occur upon irradiation. Thus, photoswitch design should focus on maximizing the free energy difference between the dark and light states and then suitably poising the system in the dark state.

Changes in the fractional occupancy of a regulatory binding site may be expected to lead to changes in gene expression levels. Changes of only 2- or 3-fold in gene expression level are sometimes associated with clear differences in phenotype (*32*−*34*), so that genetically encoded photochemical tools that would permit 10−100-fold changes in gene expression associated with AP-1 regulatory sites could be of substantial use, particularly for studies of the role of AP-1-dependent gene expression in cell proliferation, tumorogenesis, differentiation, and apoptosis (*35*−*37*).

REFERENCES

1. Deiters, A. (2009) Light activation as a method of regulating and studying gene expression. *Curr. Opin. Chem. Biol. 13*, 678–686.
2. Liu, Y., He, Q., and Cheng, P. (2003) Photoreception in *Neurospora*: A tale of two White Collar proteins. *Cell. Mol. Life Sci. 60*, 2131–2138.
3. Takahashi, F., Yamagata, D., Ishikawa, M., Fukamatsu, Y., Ogura, Y., Kasahara, M., Kiyosue, T., Kikuyama, M., Wada, M., and Kataoka, H. (2007) AUREOCHROME, a photoreceptor required for photomorphogenesis in stramenopiles. *Proc. Natl. Acad. Sci. U.S.A. 104*, 19625–19630.
4. Shimizu-Sato, S., Huq, E., Tepperman, J. M., and Quail, P. H. (2002) A light-switchable gene promoter system. *Nat. Biotechnol. 20*, 1041–1044.
5. Yazawa, M., Sadaghiani, A. M., Hsueh, B., and Dolmetsch, R. E. (2009) Induction of protein-protein interactions in live cells using light. *Nat. Biotechnol. 27*, 941–945.
6. Strickland, D., Moffat, K., and Sosnick, T. R. (2008) Light-activated DNA binding in a designed allosteric protein. *Proc. Natl. Acad. Sci. U.S.A. 105*, 10709–10714.
7. Strickland, D., Yao, X., Gawlak, G., Rosen, M. K., Gardner, K. H., and Sosnick, T. R. (2010) Rationally improving LOV domain-based photoswitches. *Nat. Methods 7*, 623–626.
8. Morgan, S. A., Al-Abdul-Wahid, S., and Woolley, G. A. (2010) Structure-based design of a photocontrolled DNA binding protein. *J. Mol. Biol. 399*, 94–112.
9. Yin, S., Ding, F., and Dokholyan, N. V. (2010) Computational evaluation of protein stability change upon mutations. *Methods Mol. Biol. 634*, 189–201.
10. Das, R., and Baker, D. (2008) Macromolecular modeling with Rosetta. *Annu. Rev. Biochem. 77*, 363–382.
11. Devanathan, S., Genick, U. K., Getzoff, E. D., Meyer, T. E., Cusanovich, M. A., and Tollin, G. (1997) Preparation and properties of a 3,4-dihydroxycinnamic acid chromophore variant of the photoactive yellow protein. *Arch. Biochem. Biophys. 340*, 83–89.
12. Changenet-Barret, P., Espagne, A., Charier, S., Baudin, J. B., Jullien, L., Plaza, P., Hellingwerf, K. J., and Martin, M. M. (2004) Early molecular events in the photoactive yellow protein: Role of the chromophore photophysics. *Photochem. Photobiol. Sci. 3*, 823–829.
13. Fersht, A. (1999) Structure and mechanism in protein science, W. H. Freeman, New York.
14. Clarke, J., and Fersht, A. R. (1993) Engineered disulfide bonds as probes of the folding pathway of barnase: Increasing the stability of proteins against the rate of denaturation. *Biochemistry 32*, 4322–4329.
15. Getzoff, E. D., Gutwin, K. N., and Genick, U. K. (2003) Anticipatory active-site motions and chromophore distortion prime photoreceptor PYP for light activation. *Nat. Struct. Biol. 10*, 663–668.
16. Dehouck, Y., Grosfils, A., Folch, B., Gilis, D., Bogaerts, P., and Rooman, M. (2009) Fast and accurate predictions of protein stability changes upon mutations using statistical potentials and neural networks: PoPMuSiC-2.0. *Bioinformatics 25*, 2537–2543.
17. Gilis, D., and Rooman, M. (2000) PoPMuSiC, an algorithm for predicting protein mutant stability changes: Application to prion proteins. *Protein Eng. 13*, 849–856.
18. Gonzalez, L., Jr., Woolfson, D. N., and Alber, T. (1996) Buried polar residues and structural specificity in the GCN4 leucine zipper. *Nat. Struct. Biol. 3*, 1011–1018.
19. Ellenberger, T. E., Brandl, C. J., Struhl, K., and Harrison, S. C. (1992) The GCN4 basic region leucine zipper binds DNA as a dimer of uninterrupted α helices: Crystal structure of the protein-DNA complex. *Cell 71*, 1223–1237.
20. Mason, J. M., and Arndt, K. M. (2004) Coiled coil domains: Stability, specificity, and biological implications. *ChemBioChem 5*, 170–176.
21. Imamoto, Y., Tatsumi, S., Harigai, M., Yamazaki, Y., Kamikubo, H., and Kataoka, M. (2008) Diverse roles of glycine residues conserved in photoactive yellow proteins. *Biophys. J. 94*, 3620–3628.
22. Hoersch, D., Otto, H., Joshi, C. P., Borucki, B., Cusanovich, M. A., and Heyn, M. P. (2007) Role of a conserved salt bridge between the PAS core and the N-terminal domain in the activation of the photoreceptor photoactive yellow protein. *Biophys. J. 93*, 1687–1699.
23. Dantas, G., Kuhlman, B., Callender, D., Wong, M., and Baker, D. (2003) A large scale test of computational protein design: Folding and stability of nine completely redesigned globular proteins. *J. Mol. Biol. 332*, 449–460.
24. Yin, S., Ding, F., and Dokholyan, N. V. (2007) Eris: An automated estimator of protein stability. *Nat. Methods 4*, 466–467.
25. Yin, S., Ding, F., and Dokholyan, N. V. (2007) Modeling backbone flexibility improves protein stability estimation. *Structure 15*, 1567–1576.
26. Philip, A. F., Eisenman, K. T., Papadantonakis, G. A., and Hoff, W. D. (2008) Functional tuning of photoactive yellow protein by active site residue 46. *Biochemistry 47*, 13800–13810.
27. Lee, B. C., and Hoff, W. D. (2008) Proline 54 trans-cis isomerization is responsible for the kinetic partitioning at the last-step photocycle of photoactive yellow protein. *Protein Sci. 17*, 2101–2110.
28. Harigai, M., Yasuda, S., Imamoto, Y., Yoshihara, K., Tokunaga, F., and Kataoka, M. (2001) Amino acids in the N-terminal region regulate the photocycle of photoactive yellow protein. *J. Biochem. 130*, 51–56.
29. Bernard, C., Houben, K., Derix, N. M., Marks, D., van der Horst, M. A., Hellingwerf, K. J., Boelens, R., Kaptein, R., and van Nuland, N. A. (2005) The solution structure of a transient photoreceptor intermediate: Δ25 photoactive yellow protein. *Structure 13*, 953–962.
30. Woolley, G. A., Jaikaran, A. S., Berezovski, M., Calarco, J. P., Krylov, S. N., Smart, O. S., and Kumita, J. R. (2006) Reversible photocontrol of DNA binding by a designed GCN4-bZIP protein. *Biochemistry 45*, 6075–6084.
31. Meyer, T. E., Yakali, E., Cusanovich, M. A., and Tollin, G. (1987) Properties of a water-soluble, yellow protein isolated from a halophilic phototrophic bacterium that has photochemical activity analogous to sensory rhodopsin. *Biochemistry 26*, 418–423.
32. Antony, A. K., Kong, W., and Lorenz, H. P. (2010) Upregulation of neurodevelopmental genes during scarless healing. *Ann. Plast. Surg. 64*, 247–250.

33. Jais, P. H. (2005) How frequent is altered gene expression among susceptibility genes to human complex disorders? *Genet. Med. 7*, 83–96.
34. Samaco, R. C., Fryer, J. D., Ren, J., Fyffe, S., Chao, H. T., Sun, Y., Greer, J. J., Zoghbi, H. Y., and Neul, J. L. (2008) A partial loss of function allele of methyl-CpG-binding protein 2 predicts a human neurodevelopmental syndrome. *Hum. Mol. Genet. 17*, 1718–1727.
35. Lopez-Bergami, P., Lau, E., and Ronai, Z. (2010) Emerging roles of ATF2 and the dynamic AP1 network in cancer. *Nat. Rev. Cancer 10*, 65–76.
36. Wagner, E. F. (2002) Functions of AP1 (Fos/Jun) in bone development. *Ann. Rheum. Dis. 61* (Suppl. 2), ii40–ii42.
37. Karin, M., and Gallagher, E. (2005) From JNK to pay dirt: jun kinases, their biochemistry, physiology and clinical importance. *IUBMB Life 57*, 283–295.